THE JOURNAL OF BIOLOGICAL CHEMISTRY VOL. 286, NO. 22, pp. 19917–19931, June 3, 2011

In Vivo Crystallization of Human IgG in the Endoplasmic Reticulum of Engineered Chinese Hamster Ovary (CHO) Cells[S]

Received for publication, November 18, 2010, and in revised form, March 26, 2011 Published, JBC Papers in Press, April 4, 2011, DOI 10.1074/jbc.M110.204362

Haruki Hasegawa[‡1], John Wendling[§], Feng He[¶], Egor Trilisky[‖], Riki Stevenson[**], Heather Franey[**], Francis Kinderman[**], Gary Li[**], Deirdre Murphy Piedmonte[**], Timothy Osslund[‡‡], Min Shen[‡], and Randal R. Ketchem[‡]

From the Departments of [‡]Protein Science, [§]Cell Sciences and Technologies, [¶]Formulation and Analytical Resources, and [‖]Purification Process Development, Amgen Inc., Seattle, Washington 98119 and the Departments of [**]Formulation and Analytical Resources and [‡‡]Analytical and Formulation Sciences, Amgen Inc., Thousand Oaks, California 91320

Protein synthesis and secretion are essential to cellular life. Although secretory activities may vary in different cell types, what determines the maximum secretory capacity is inherently difficult to study. Increasing protein synthesis until reaching the limit of secretory capacity is one strategy to address this key issue. Under highly optimized growth conditions, recombinant CHO cells engineered to produce a model human IgG clone started housing rod-shaped crystals in the endoplasmic reticulum (ER) lumen. The intra-ER crystal growth was accompanied by cell enlargement and multinucleation and continued until crystals outgrew cell size to breach membrane integrity. The intra-ER crystals were composed of correctly folded, endoglycosidase H-sensitive IgG. Crystallizing propensity was due to the intrinsic physicochemical properties of the model IgG, and the crystallization was reproduced *in vitro* by exposing a high concentration of IgG to a near neutral pH. The striking cellular phenotype implicated the efficiency of IgG protein synthesis and oxidative folding exceeded the capacity of ER export machinery. As a result, export-ready IgG accumulated progressively in the ER lumen until a threshold concentration was reached to nucleate crystals. Using an *in vivo* system that reports accumulation of correctly folded IgG, we showed that the ER-to-Golgi transport steps became rate-limiting in cells with high secretory activity.

Immunoglobulins continue to serve as an important model secretory cargo for investigating biochemical processes of oxidative protein folding and subunit assembly in the ER[2] lumen (1). Although immunoglobulins are indispensable as research tools, their potential as human therapeutics has attracted significant interest in recent years in the manufacture of human IgG at large scale (2, 3). Therapeutic human IgGs are often recombinantly produced in variants of CHO cells that were adapted to propagate in suspension culture format. Mammalian cell hosts are often preferred for biopharmaceutical production not only just to achieve desired co-translational and post-translational modifications (4) but also to exploit the stringent protein quality control mechanisms that only allow the secretion of properly folded and correctly assembled proteins (5, 6).

To achieve high recombinant protein expression levels in mammalian cells, various *cis*-acting exogenous nucleotide elements have been engineered into transgene expression cassettes to enhance transcription efficiency, extend message half-life, and increase translation initiation frequency (7, 8). Exogenous nucleotide elements also enabled strategies to increase transgene copy number by gene amplification and to suppress epigenetic silencing (9–12). Despite the success in boosting protein expression *per se* through these expression vector engineering approaches, such enhancements did not translate into higher glycoprotein secretion partly because post-translational events such as protein folding/assembly and intracellular vesicular transport steps along the secretory organelles became the new bottlenecks (13–15). To alleviate such post-translational bottlenecks, various approaches were evaluated to enhance the protein secretion efficiency. Advancements in cell phenotype engineering, metabolic engineering, systems approach, growth medium optimization, and bioreactor technology have all culminated in explosive increases in the production titers of therapeutic human IgGs in recent years (16–19).

At the cellular level, protein secretion capacity may be thought of as the cumulative efficiency of numerous biochemical reactions and biomechanical steps constituting the biosynthetic secretory pathway. Even if cells expand their capacity by increasing the number of participating catalytic machines (*e.g.* enzymes and mechanoenzymes) and the frequency of catalytic events, there will eventually be a physical limit that determines the ceiling of secretory capacity, namely how much energy to generate and expend as well as how many proteins to synthesize, fold, assemble, package, traffic, and secrete by individual cells in a given time and space. Just as different enzyme-substrate relationships are different from one another, the physical secretory capacity for a given cell may be different, for instance, depending on which particular human IgG clones are synthesized and trafficked because each IgG clone has unique VH and

[S] The on-line version of this article (available at http://www.jbc.org) contains Supplements 1–5.

[1] To whom correspondence should be addressed: Amgen, Inc., 1201 Amgen Court West, Seattle, WA 98119. Tel.: 206-265-7209; Fax: 206-217-0346; E-mail: harukih@amgen.com.

[2] The abbreviations used are: ER, endoplasmic reticulum; CDR, complementarity-determining region; DIC, differential interference contrast; eIF2α, eukaryotic initiation factor 2α; Fv, variable fragment; HC, heavy chain; LC, light chain; PERK, pancreatic endoplasmic reticulum eIF2α kinase; VH, variable domain of heavy chain; VL, variable domain of light chain; Bis-Tris, 2-[bis(2-hydroxyethyl)amino]-2-(hydroxymethyl)propane-1,3-diol; PNS, postnuclear supernatant; BLAST, Basic Local Alignment Search Tool; UPR, unfolded protein response; endo H, endoglycosidase H; BFA, brefeldin A.

VL sequences that determine the unique physicochemical properties of individual IgG clones. Increasing secretory protein synthesis to the point where the limit of secretory capacity is reached may be one strategy to address the key issues of cellular secretory capacities. However, it is difficult, in practice, to design effective experiments to determine the maximum capacity of the cell or what the rate-limiting step would be at that maximum.

In this study, we report detailed biochemical and biophysical characterizations of a model human IgG that caused a striking cellular phenotype that in turn provided important insights into the maximum cellular secretory capacity and rate-limiting secretory bottlenecks. In the recombinant CHO cells we engineered to overexpress a model human IgG clone, properly assembled and correctly folded IgG progressively accumulated in the ER lumen until, and even after, the solubility limit of the IgG was reached to nucleate IgG crystals. After the crystal nucleation in the ER lumen, cells apparently stopped carrying out cytokinesis, whereas the cell volume growth and karyokinesis continued. Newly folded IgG continued to feed the growth of crystals in the ER until they grew longer than the diameters of the cells and eventually punctured the cell membranes. Intra-ER crystallization required both the unique physicochemical properties of the model IgG and the biosynthetic and protein folding efficiency of the recombinant CHO cells that exceeded the ER export capacity under optimized cell culture conditions. Our study suggested that, in addition to the intrinsic limitation in intracellular protein trafficking efficiency, physicochemical properties of the secretory cargo itself play critical roles in determining the ceiling of cellular secretory capacity.

EXPERIMENTAL PROCEDURES

Detection Antibodies—Mouse anti-GM130, mouse anti-BiP, mouse anti-protein-disulfide isomerase, and mouse anti-calreticulin were from BD Transduction Laboratories. Rabbit anti-GPP130 was from Covance. Rabbit anti-calnexin was from Sigma-Aldrich. Goat anti-human IgG γ chain and goat anti-human IgG κ chain antibodies were from SouthernBiotech. Affinity-purified rabbit anti-human IgG (HC + LC) was from Jackson ImmunoResearch Laboratories. Mouse anti-GAPDH and rabbit anti-transferrin receptor were from Chemicon. Mouse anti-β-tubulin (clone E7) was from a hybridoma bank. Mouse anti-ERp57 and anti-phospho-PERK (Thr-981) were from Santa Cruz Biotechnology. Rabbit anti-PERK, rabbit anti-eIF2α, and rabbit anti-phospho-eIF2α were from Cell Signaling Technology. Mouse anti-XBP1 was from R&D Systems. Mouse anti-ATF6α (clone 4H18) was from United States Biological.

Cell Line Development—The VH and VL sequences of our model human IgG were subcloned into a pair of human IgG expression vectors that allow a stable chromosomal integration and gene amplification by genetically linking the HC and LC coding sequences to dihydrofolate reductase selection markers (20). Expression vectors were introduced to dihydrofolate reductase-deficient CHO cells (21) by electroporation. Stable integrants were selected by culturing the cells in a growth medium devoid of glycine, hypoxanthine, and thymidine. The recovered resistant cell population was cultured in the presence of up to 500 nM methotrexate in a serum-free, chemically defined cell culture medium (21). A clonal line was derived from the gene-amplified pool by a limiting dilution method.

CHO Cell Cultivation and IgG Production—The engineered clonal CHO cell line was maintained in shaker flasks in a humidified incubator at 36 °C, 5% CO_2 on a shaker platform using an animal component-free, chemically defined CHO cell culture medium optimized in our laboratories. Cells were then inoculated into a 50-liter CultiBag RM (Sartorius) and cultivated using a BIOSTAT® platform (Sartorius) at 36 °C, pH 7.1, 30% dissolved oxygen. Nutrition-balanced feeds were added to the cell culture as needed depending on the nutrient depletion levels. Cell viability, cell density, medium pH, osmolality, antibody titer, etc. were monitored daily during a 16-day cell cultivation period. Cell culture medium was harvested using a Millistak+ HC Pod Filter (Millipore), a Zeta Plus® BioCap™ filter (CUNO Inc.), and a Sartopore 2® filter (Sartorius). Using a post-filtration cell culture medium, the expression titer of human IgG in the harvested medium was determined by using POROS® A20 analytical HPLC column (Applied Biosystems).

Recombinant Protein Production Using Transiently Transfected HEK293 Cells—HEK293-EBNA1 cells and the expression vector pTT5 were obtained from Dr. Yves Durocher (National Research Council of Canada). Methods for serum-free suspension cell culture and transfection were described previously (22). In brief, cells were cultured in Freestyle™ 293 medium (Invitrogen) in suspension format using shaker flasks placed on a shaker platform rotating at 150 rpm in a humidified incubator at 37 °C, 5% CO_2. Cell culture medium was harvested on day 6 post-transfection for protein purification and other analyses.

IgG Purification—Human IgG was first purified from harvested cell culture medium by protein A affinity chromatography using MabSelect resin (GE Healthcare) according to the manufacturer's instructions. Eluted IgG was subjected to cation exchange chromatography using Fractogel SO_3^- (M) resin (EDM Chemicals) according to the manufacturer's protocol. The elution fractions containing IgG were pooled and purified by hydrophobic interaction resin using phenyl-Sepharose 6 Fast Flow (GE Healthcare). The purified human IgG was concentrated and buffer-exchanged by tangential flow filtration to an acidic buffer (10 mM acetate, 0.26 M sucrose (pH 5.2)), which hereafter will be referred to as acetate buffer.

Isolation of Intracellular Crystals—On day 5, CHO cells were withdrawn from CultiBag culture vessel and collected by low speed centrifugation (1,000 × *g*, 5 min). The cell pellets were lysed in PBS (pH 7.2) containing 1% Triton X-100 for 10 min on ice followed by low speed centrifugation. Collected crystals were washed in PBS (pH 7.2) three times by repeating the low speed centrifugation steps to remove contaminating cytosolic proteins and detergent-extracted membrane-anchored proteins. The total dilution factor of the washing step was 1:420,000. The quality of isolated crystals was visually inspected by microscopy before they were allowed to dissolve fully in PBS (pH 7.2) by incubating on ice for 3 h. Any insoluble components such as extracted nuclei were subsequently removed by centrifugation (15,000 × *g*, 15 min). The resulting supernatant was directly used in protein identification experiments by mass

spectrometry (not shown) or deglycosylation experiments (below) or further purified by protein A affinity resin MAbSuRe (GE Healthcare) in a batch method. A pool of the IgG-containing fraction was buffer-exchanged to acetate buffer.

Peptide:N-Glycosidase F and Endoglycosidase H Treatment—Purified secreted IgG and the fully dissolved crystal-derived IgG (before protein A affinity purification) were treated with peptide:*N*-glycosidase F (New England Biolabs) or endoglycosidase H (New England Biolabs) according to the manufacturer's protocol. Enzyme-treated IgGs were resolved by SDS-PAGE under reducing conditions followed by Western blotting analysis.

Western Blotting—SDS-PAGE was performed using an Invitrogen NuPAGE® 4–12% Bis-Tris gradient gel and a compatible buffering system. The reducing condition contained 5% β-mercaptoethanol (final) in the sample buffer. The non-reducing condition was without reducing agents but contained 2 mM *N*-ethylmaleimide (final) as an alkylating agent. Resolved proteins were electrotransferred to a nitrocellulose membrane, blocked with Odyssey blocking buffer (LI-COR Biosciences), and probed with suitable primary antibodies. After washing steps in PBS containing 0.05% Tween 20, the nitrocellulose membranes were treated with Alexa Fluor® 680-conjugated secondary antibodies (Invitrogen). The membranes were scanned, and the images were acquired by using the Odyssey infrared imaging system (LI-COR Biosciences).

Immunofluorescence Microscopy—Suspension-cultured CHO cells were withdrawn from the CultiBag via a sampling portal on day 5 or 6 and seeded onto polylysine-coated glass coverslips using DMEM/F-12 medium (Invitrogen) supplemented with 10% FBS. After 24 h of static culture, cells were fixed with 4% paraformaldehyde in 0.1 M sodium phosphate (pH 7.2) for 30 min at room temperature. After washing steps in PBS containing 0.1 M glycine, the fixed cells were incubated with permeabilization buffer (PBS containing 0.4% saponin, 1% BSA, 5% fish gelatin) for 15 min followed by incubation with primary antibody in permeabilization buffer for 60 min. After three washes in permeabilization buffer, the cells were incubated with Alexa Fluor 488- or 594-conjugated secondary antibodies in permeabilization buffer for 60 min. Slides were analyzed using a Nikon Eclipse 80i microscope using a 100×, 60×, or 40× CFI Plan apochromatic oil objective lens and a Chroma FITC-HYQ or Texas Red-HYQ filter. Images were acquired using a Cool SNAP HQ2 digital camera (Photometrics) and Nikon Elements Basic Research imaging software.

Homogenization and Fractionation—Using engineered CHO cells maintained in shaker flasks, cells were collected by low speed centrifugation (1,000 × *g*, 5 min), resuspended in a hypotonic buffer (10 mM Hepes, 18 mM potassium acetate (pH 7.2)), and incubated on ice for 10 min. Treated cells were spun down as before and resuspended in homogenization buffer (10 mM Hepes, 0.26 M sucrose, 2 mM EGTA, 2 mM EDTA (pH 7.2)) supplemented with Complete™ protease inhibitor mixture (Roche Applied Science). Cells were homogenized in a glass Dounce homogenizer (~20 strokes), and the postnuclear supernatant (PNS) was collected after 5 min of centrifugation at 1,000 × *g*. The PNS was then centrifuged at 100,000 × *g* for 60 min to separate the soluble fraction (cytosol) from the particulate fraction (membrane-bound organelles). The PNS, cytosol, and particulate fractions were analyzed by Western blotting.

Differential Scanning Calorimetry—A MicroCal VP-Capillary differential scanning calorimetry system (GE Healthcare) equipped with an autosampler was used to assess protein conformational stability and folding of both secreted IgG and crystal-derived IgG according to a method described previously (23). Briefly, IgG samples were analyzed at 0.5 mg/ml in acetate buffer (pH 5.2), and the blank acetate buffer solution was measured for base-line subtraction. Solution reference and protein samples were measured in a 135-μl cell from 20 to 110 °C at a heating rate of 60 °C/h. The heat capacity during protein melting was calculated by normalizing over protein concentration.

In Vitro pH Shock Experiment—Purified IgG (105 mg/ml in acetate buffer (pH 5.2)) was mixed with [1.5/100] volume of 1 M citrate (pH 7.0) in a glass vial. After a gentle mixing, the glass vial was statically incubated at room temperature for 24 h. Precipitates were collected and subjected to DIC microscopy using a 40× oil objective lens. The concentration of IgG that remained soluble in the aqueous phase was determined by absorbance at 280-nm wavelength using a specific extinction coefficient. In a different experiment, the same IgG stock was dialyzed against PBS (pH 7.2) at 4 °C for 18 h. Precipitates were collected and visualized using a bright field microscope with 10× dry objective lens.

Viscosity Measurement—Viscosity (in centipoises) of purified IgG (~150 mg/ml in acetate buffer (pH 5.2)) was measured at 25 °C with an LV-DVIII Cone/Plate viscometer (Brookfield Engineering) using a CP-40 spindle and its sample cup according to the manufacturer's instructions. Viscosity measurements at various shear rates were averaged to report one viscosity value per sample at the IgG concentration used.

Raman Spectroscopy—IgG crystals generated by the *in vitro* pH shock procedures (mentioned above) or the intracellular IgG crystals in paraformaldehyde-fixed intact cells were stabilized onto gold-coated filters (Bruker Optics). The Raman spectra were measured directly on the filter, from 70 to 4,000 cm^{-1}, using the Senterra® Raman microscope spectrometer (Bruker Optics) with a green 532 nm laser. Each spectrum was collected at the resolution of ~12 cm^{-1} using a 20× objective lens and 50 × 1,000-μm aperture.

Structural Modeling of IgG Variable Fragment (Fv)—To select a suitable Fv framework template, individual chains of our model IgG were BLAST (24)-searched against the Protein Data Bank (25) by excluding Kabat-defined CDRs (26) to look for Fv structure with the highest sequence identity but with minimum interchain interface violations. The individual CDRs were then used to search the Protein Data Bank to find the CDR structure template from all known antibody structures that match in length to the query CDRs. The best template was selected on the basis of highest identity to the query CDR, structural resolution, and B-factors of the templates. The chosen template CDRs were placed onto the chosen Fv framework by superposition of the Cα carbons from the three residues on either side of each CDR. A final homology model was built from this template using the Molecular Operating Environment (Chemical Computing Group, Montreal, Canada).

RESULTS

Formation of Rod-shaped Crystals in Cytoplasm of Recombinant CHO Cells Overexpressing Human IgG—To express transgenes encoding our model human IgG protein, a stable CHO cell line was developed by using a pair of expression vectors with a promoter/enhancer element from human cytomegalovirus immediate-early gene and the expression-augmenting sequence elements that will allow a sustained high level transcription (20). The vector pair allows the selection of stable transfectants that received both HC- and LC-encoding expression vectors by widely used amplifiable dihydrofolate reductase selection markers. The copy number of stably integrated transgene was amplified by exposing the cells to up to 500 nM methotrexate. Using the established clonal CHO cell line, we first determined how much human IgG can be secreted to the culture medium over a 16-day period using a chemically defined culture medium in a disposable 50-liter cell culture bag. During the prolonged cell cultivation, culture medium pH was controlled to maintain a pH of ~7.1 (Supplement 1A). The maximum viable cell density (20×10^6 cells/ml) was reached on day 8 (Supplement 1B), and the cell viability started decreasing at around day 9 (Supplement 1C). Cell doubling time was ~28 h at day 1 and ~46 h by day 6. Daily monitoring of osmolality showed that during the first 7 days of cell cultivation, when all of our cellular characterization studies were performed (see below), the osmolality was stable in the range of 300–400 mOsm/kg (data not shown). At the end of the 16-day cell culture, recovered IgG from the culture medium reached 4.14 g/liter. Specific productivity (qP) calculated on day 16 was ~35 pg of IgG/cell/day (or $\sim 1 \times 10^8$ IgG/cell/min). During the cell cultivation, not only did we observe a high prevalence of enlarged cells but also the growth of rod-shaped crystals in a number of cells (Fig. 1*A*). The normal cell diameter of suspension-cultured CHO cells is typically 10–15 μm, but in many instances, the size of the cells reached 50 μm in diameter by day 5. Furthermore, the crystal elongation appeared to exceed the cell size growth. As a result, the crystals created membrane tension that deformed spherical suspension CHO cells into various "football" shapes (Fig. 1*B* and Supplement 2). To make a more detailed morphological observation of the intracellular rods, suspension-cultured CHO cells were allowed to adhere and spread on glass coverslips. Once laid down on a flat surface, it became evident that many enlarged rod-harboring cells were multinucleated and that individual cells often housed multiple crystals in the cytoplasm (Fig. 1*C* and Supplement 3). By analyzing the images of crystal-harboring cells at multiple Z-sections, it was evident that the rod-shaped crystals resided in the cytoplasmic space (Fig. 2 and Supplement 4).

Intracellular Crystals Are Housed in ER—Crystal formation in mammalian cells is not unprecedented. In one instance, crystals were made of cholesterol in bovine artery endothelial cells of atherosclerotic lesions (27). In another example, crystals developed in the corneal epithelia of tyrosine-fed rats that mimic the human metabolic disorder tyrosinosis, and the crystals were made up of tyrosine amino acid (28). To obtain clues to the identity of crystals in recombinant CHO cells, we first examined whether the crystals are associated with any particular organelles. Among the various organelle markers tested, calnexin-positive ER membranes clearly encapsulated the entire rod-shaped crystals regardless of the number of crystals in a given cell (Fig. 3). A cis-Golgi marker, GM130 (Fig. 3), and other markers of the endomembrane system including endosomes and lysosomes as well as mitochondria showed no association with the crystals or did not result in the crystal-encapsulating staining pattern (data not shown). The crystals thus clearly formed and grew in the ER lumen of CHO cells.

Model IgG Accumulates in ER during Its Biosynthesis—To determine which trafficking step or organelle is rate-limiting in the model IgG biosynthesis and secretion, we performed immunofluorescence microscopy to visualize the steady-state subcellular localization of itinerant human IgG within the secretory pathway. Using both anti-γ heavy chain and anti-κ light chain antibodies, we found a significant accumulation of human IgG in the ER lumen (Fig. 4, *A* and *B*). The morphology of the ER remained tubular and reticular (Fig. 4*B*, *panel g*) instead of developing a stacked sheet ER morphology, which is frequently observed in professional secretory cells such as pancreatic β-cells and IgG-secreting plasma cells (29, 30). Furthermore, compared with the cells already developing crystals, the cells that had yet to nucleate crystals had qualitatively higher intra-ER concentrations of IgG as evidenced by the stronger anti-IgG (HC + LC) staining signals (Fig. 5, marked by *asterisks*). Although there were inevitable cell-to-cell variations in protein expression levels among cells in this clonal population (addressed in "Discussion"), the staining signal differences between crystal-housing and non-crystal-forming cells were consistent, and the difference was evident when these cells were placed next to each other (Fig. 5). Because the fluorescent signal strengths from crystal-harboring and non-crystal-harboring cells were so widely apart, we could not bring both signals simultaneously within a linear detection range; it was thus difficult to quantitatively display the apparent signal differences. Because the antisera were affinity-purified to detect epitopes presented by the folded and/or assembled IgG species, our results were likely to suggest a higher accumulation of export-ready IgG as well as folding IgG within the cells that have yet to develop crystals. This observation prompted us to hypothesize that, although we initially thought it was quite unlikely, the crystals are composed of human IgG, the overexpressed secretory cargo itself. If our hypothesis is correct, the model would predict that 1) the intra-ER IgG accumulation reaches the highest concentration just before the crystal nucleation, 2) once the crystals nucleate, molecular crowding in the ER lumen will be alleviated because the crystals absorb existing and newly folded IgG to fuel crystal growth, and 3) crystal growth competes with ER export machinery for the supply of newly folded, export-ready IgG in the ER lumen; thus, it reduces the specific productivity.

Intra-ER Crystals Are Composed of Properly Assembled Human IgG—ER sometimes accumulates unfolded and misfolded secretory proteins that often cause ER stress and activate "unfolded protein response (UPR)" signaling pathways trying to cope with the protein folding demand, to re-establish ER homeostasis, and sometimes to induce apoptosis when protein folding problems are not satisfactorily addressed (31). Because dis-

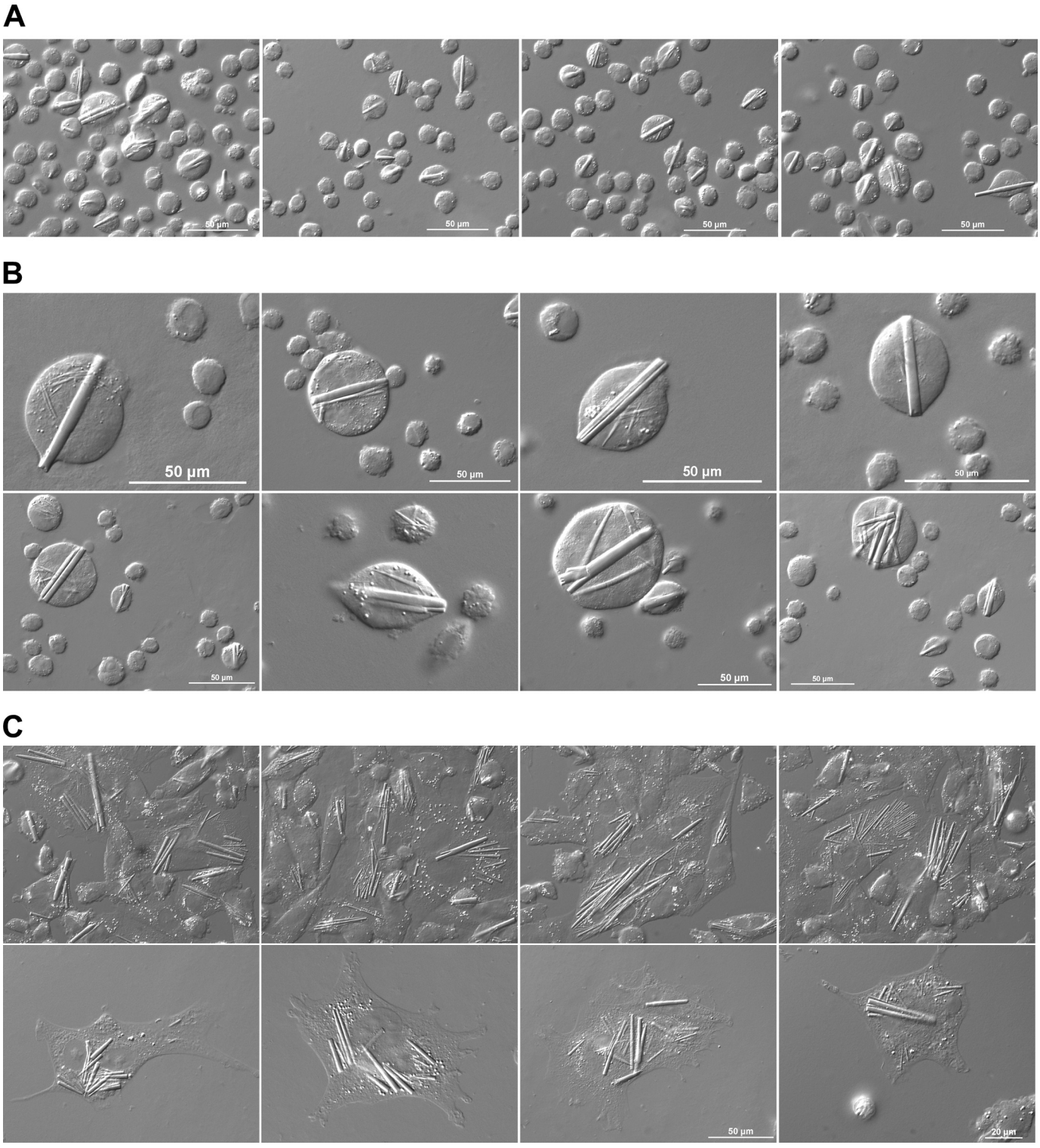

FIGURE 1. **Rod-shaped crystals develop in CHO cells overexpressing recombinant human IgG.** *A* and *B*, suspension-cultured CHO cells were withdrawn from a 50-liter bioreactor bag on day 5 and immobilized on 3-triethoxysilylpropylamine-coated glass coverslips. Cells were paraformaldehyde-fixed and visualized using a DIC microscope. *Scale bars*, 50 μm. *C*, suspension-cultured CHO cells were seeded onto polylysine-coated coverslips and statically cultured for 24 h using DMEM/F-12 medium supplemented with 10% FBS in a humidified incubator at 37 °C, 5% CO_2. Cells were paraformaldehyde-fixed and visualized using a DIC microscope. *Scale bar*, 20 or 50 μm as indicated.

ordered polypeptides may be heterogeneous and may not pack efficiently to form crystals, we hypothesized that not only are the crystals composed of human IgGs but also that they are fully folded and correctly assembled. To test this hypothesis, we isolated intracellular crystals from detergent-extracted cell lysate by taking advantage of the slow dissolving characteristics of the crystals (see "Experimental Procedures"). Visual inspection of isolated crystals revealed the presence of contaminating mem-

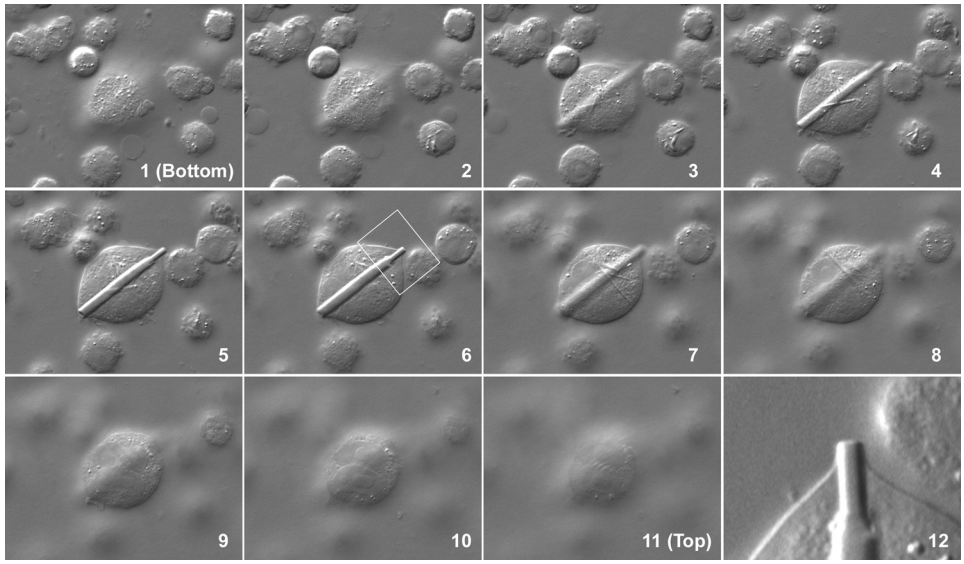

FIGURE 2. **Rod-shaped crystals are in cytoplasm.** Suspension-cultured CHO cells were stabilized on 3-triethoxysilylpropylamine-coated glass coverslips and paraformaldehyde-fixed. Cell images (*panels 1–12*) were acquired in 11 different focal planes starting from the bottom (*panel 1*) to the top (*panel 11*) of an enlarged cell. The *white boxed* area in *panel 6* is digitally cropped and magnified in *panel 12*.

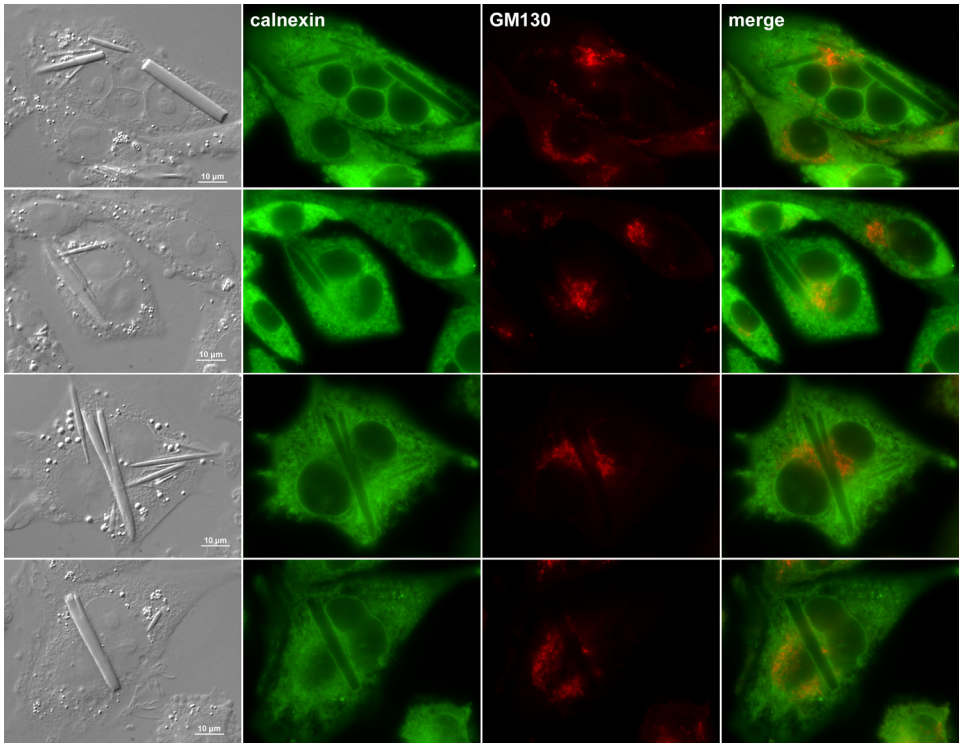

FIGURE 3. **Intracellular crystals are housed inside of ER membranes.** Suspension-cultured CHO cells were seeded on to polylysine-coated glass coverslips and cultured statically for 24 h. After paraformaldehyde fixation, cells were permeabilized and immunostained with anti-calnexin and anti-GM130 antibodies followed by labeling with suitable secondary antibodies. Stained cells were examined by using an epifluorescence microscope.

brane-extracted nuclei (Fig. 6*A*), which co-sediment with crystals during low speed centrifugation steps. After fully dissolving the crystals in PBS and removing insoluble components, the resulting supernatant was analyzed by SDS-PAGE and Western blotting (Fig. 6*B*). When examined under reducing conditions, the dissolved crystal sample contained ~25- and ~50-kDa proteins (*lane 2*) identical to the sizes of LC and HC of IgG, respectively, purified from the harvested cell culture medium (*lane 1*). It also contained an ~40-kDa protein of unknown identity (addressed below). When analyzed under non-reducing conditions, both 25- and 50-kDa bands formed an ~150-kDa band (*lane 4*), which was again identical in size to the intact IgG purified from the harvested culture medium (*lane 3*). In contrast, the mobility of the ~40-kDa protein remained unchanged under the two conditions. Western blotting using anti-human IgG showed that the 25- and 50-kDa proteins were LC and HC of human IgG, respectively (Fig. 6*B*, *right panel*). Mass spectrometric analysis revealed that the major contaminating protein

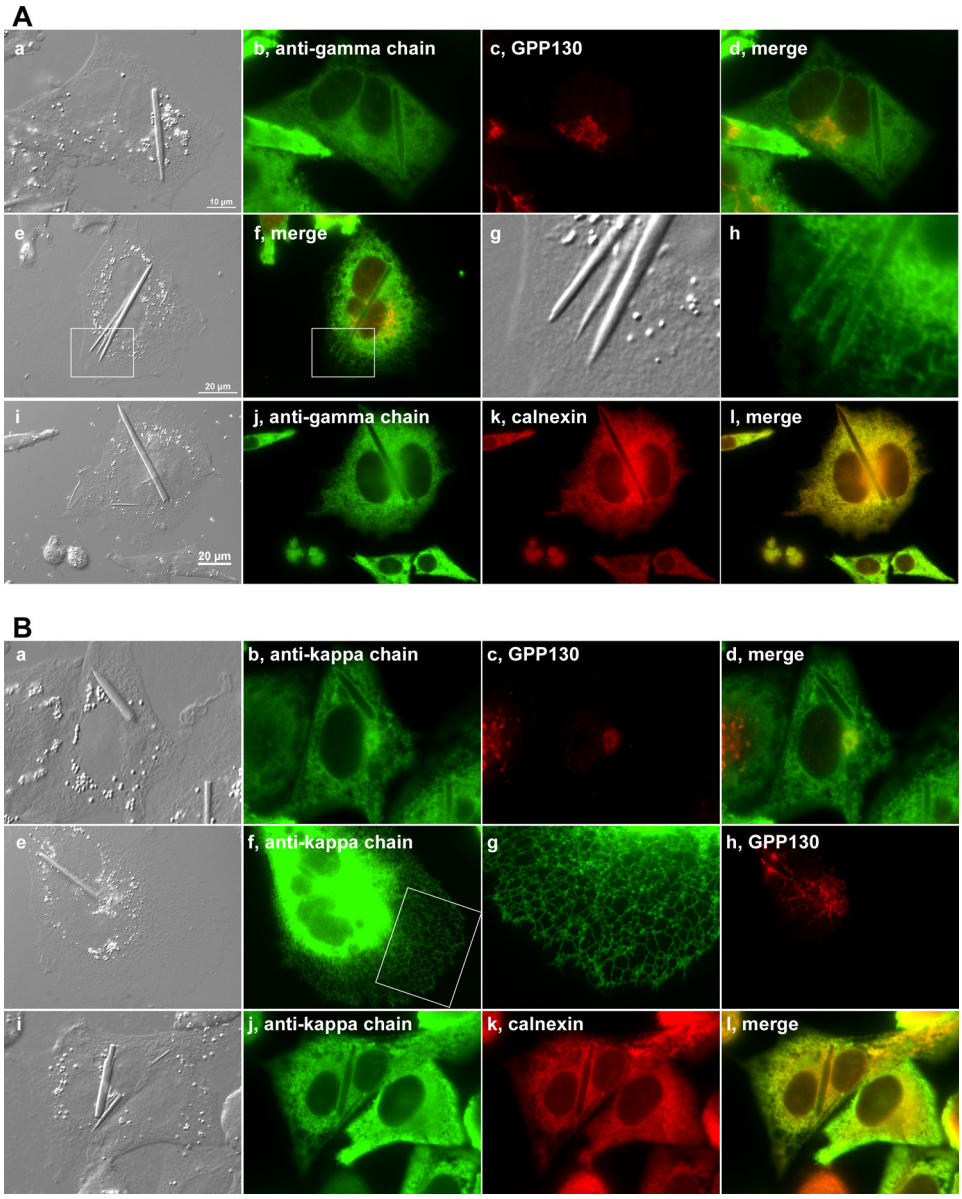

FIGURE 4. **Model IgG accumulates in ER.** Suspension-cultured cells were allowed to spread on polylysine-coated glass coverslips for 24 h before cells were fixed with paraformaldehyde. *A*, *panels a–l*, cells were stained with an anti-γ chain antibody and co-stained with an anti-GPP130 or an anti-calnexin antibody. The *white boxed* area in *panel i* is digitally cropped and enlarged in *panels k* and *l*. *B*, *panels a–l*, cells were co-stained with anti-κ chain and anti-GPP130 antibodies. The *white boxed* area in *panel f* is digitally enlarged in *panel g*.

(~40 kDa) present in the dissolved crystal preparation (*lanes 2* and *4*, marked by *asterisks*) was hamster *actin* (LC-MS/MS data not shown). Other faintly detectable proteins were also of cytosolic origin (data not shown). The intracellular crystals were thus exclusively composed of correctly assembled, intact human IgG with no free HC or LC, and there were no detectable partially or erroneously assembled intermediates. The fact that crystal-forming IgG was oxidatively assembled at the expected stoichiometry supported that crystals were formed in the oxidizing folding environment of the ER, which agreed well with our microscopy results.

Soluble Milieu of ER Lumen Contains Heterogeneous Folding Intermediates—To examine the protein quality of "non-crystal-forming" IgG species in the ER lumen, we performed a fractionation experiment as illustrated in Fig. 7*A* (see also "Experimental Procedures"). During the homogenization step using a glass Dounce homogenizer, we unavoidably damaged the rod-shaped crystals housed in the ER membranes. Nevertheless, we removed nuclei and crystals by a low speed centrifugation step (1,000 × *g*, 10 min) and recovered a PNS. The PNS was further separated into a soluble fraction (mostly cytosolic) and a particulate fraction (mostly membrane-bound organelles) via 100,000 × *g* ultracentrifugation. The resulting three fractions were analyzed to assess the protein quality of IgG by Western blotting. Under reducing conditions, both HC and LC were detected at the expected sizes (Fig. 7*B*, *top panel*, *lanes 1–3*). When examined under non-reducing conditions, in addition to the expected ~150-kDa species (Fig. 7*B*, *top panel*, *lanes 4–6*, marked by an *arrowhead*), there were mixtures of heterogeneously sized immune-positive proteins that reflected the pres-

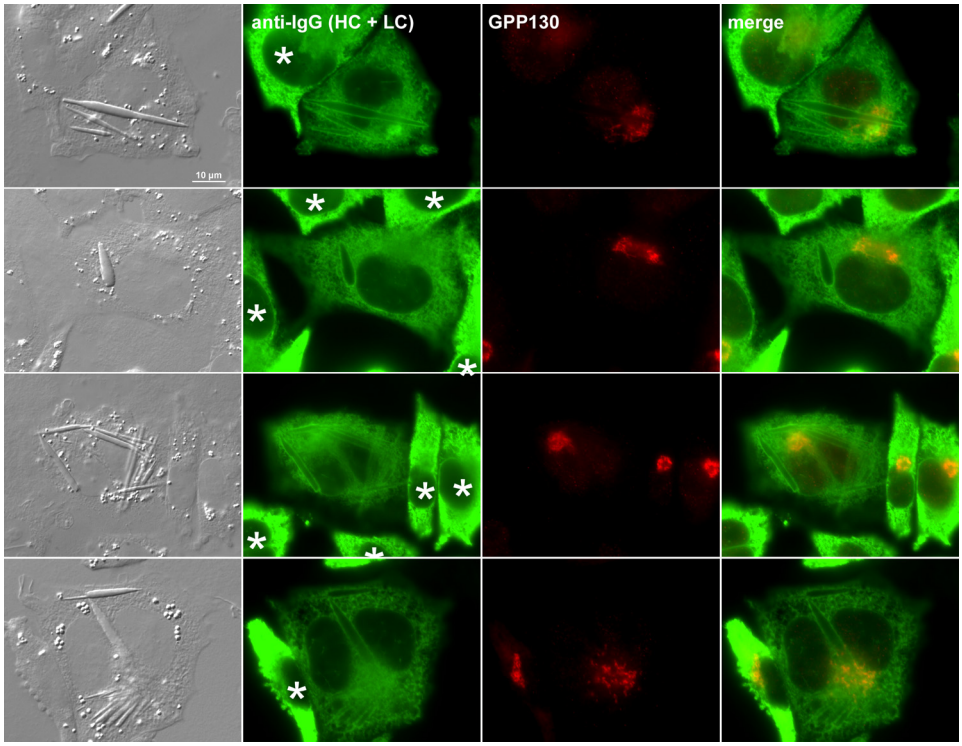

FIGURE 5. **Crystal-forming cells exhibit lower IgG concentration in ER lumen than non-crystal-forming cells.** Suspension cultured-cells were allowed to adhere on polylysine-coated glass coverslips for 24 h before cells were fixed with paraformaldehyde. Cells were co-stained with anti-human IgG (HC + LC) and anti-GPP130 antibodies. Cell images were acquired to show crystal-forming and non-crystal-forming cells in the same field. *Asterisks* are placed on the nuclei of non-crystal-forming cells.

ence of various folding intermediates and partially assembled species; some of them might be forming mixed disulfides with non-cognate partners and/or with ER-resident oxidoreductases. The soluble milieu of ER hence contained not only just the fully assembled IgG but also various folding intermediates. The faint detection of HC and LC in the cytosolic fraction is likely due to the damaging homogenization step that allowed the escape of proteins from the ER lumen rather than that they were the retrotranslocated ER-associated degradation substrates. If they were *bona fide* ER-associated degradation substrates, they were expected to be "reduced" before retrotranslocaton and polyubiquitinated after the retrotranslocation, but we did not detect such evidence.

UPR Pathways Are Activated Constitutively—Because there was a detectable amount of folding intermediates in the ER, we examined whether the UPR is activated in the IgG-overexpressing cell line. When total cell lysates prepared from equal numbers of cells were analyzed by Western blotting, PERK and its substrate eIF2α were phosphorylated in engineered CHO cells at steady state (Fig. 7*C*, *panels 7–10*). To distinguish the activation of UPR on an individual cell basis and to examine whether there is any detectable difference between crystal-housing cells and non-crystal-forming cells, we visualized the subcellular localization of endogenously expressed XBP1 and ATF6α by immunofluorescence microscopy. Judging from its subcellular localization, it was clear that pXBP1(S), which is translated from the spliced form of the XBP1 message (32, 33), accumulated in the nuclei of engineered CHO cells regardless of whether the cells housed IgG crystals (Fig. 7*D*, *left column*). Similarly, the accumulation of ATF6α in the nuclei of CHO cells (Fig. 7*D*, *right column*) indicated that the ER-anchored precursor was processed at the Golgi to liberate its soluble transcription factor domain, which then accumulated in the nuclei (34), regardless of crystal formation. As expected for cells with a high secretory activity, all three arms of UPR were constitutively activated during the cell cultivation. In good agreement with the constitutive UPR activation, when a set of major ER-resident proteins were examined by Western blotting, all the proteins tested were highly up-regulated in IgG-producing cells compared with the parental CHO cells (Fig. 7*C*, *panels 2–6*).

Crystal-forming IgG Is Folded Correctly—To determine the biochemical attributes that could differentiate intra-ER crystal IgG from the secreted counterpart, we first analyzed their *N*-linked glycan property differences. When IgGs were subjected to peptide:*N*-glycosidase F treatment, the mobility of HC shifted expectedly both in secreted and intra-ER crystal IgGs (Fig. 8*A*, *lanes 2* and *6*). The nascent heavy chains were thus properly modified with core *N*-linked glycans during co-translational ER translocation, and there was no detectable difference, or bias, in the efficiency of site occupancy between the IgG singled out to crystallize in the ER and the IgG chosen for ER exit. When the secreted IgG was treated with endoglycosidase H (endo H), there was no detectable mobility shift of its HC; thus, the core *N*-linked glycans acquired modifications in the medial Golgi during the secretory pathway trafficking (*lane 3*). In contrast, the IgG counterpart recovered from the intra-ER crystals remained sensitive to endo H treatment (*lane 7*), which clearly indicated that those IgGs were never transported out of the ER to reach the medial Golgi compartment. It also suggested that there were no aberrant events that caused the redis-

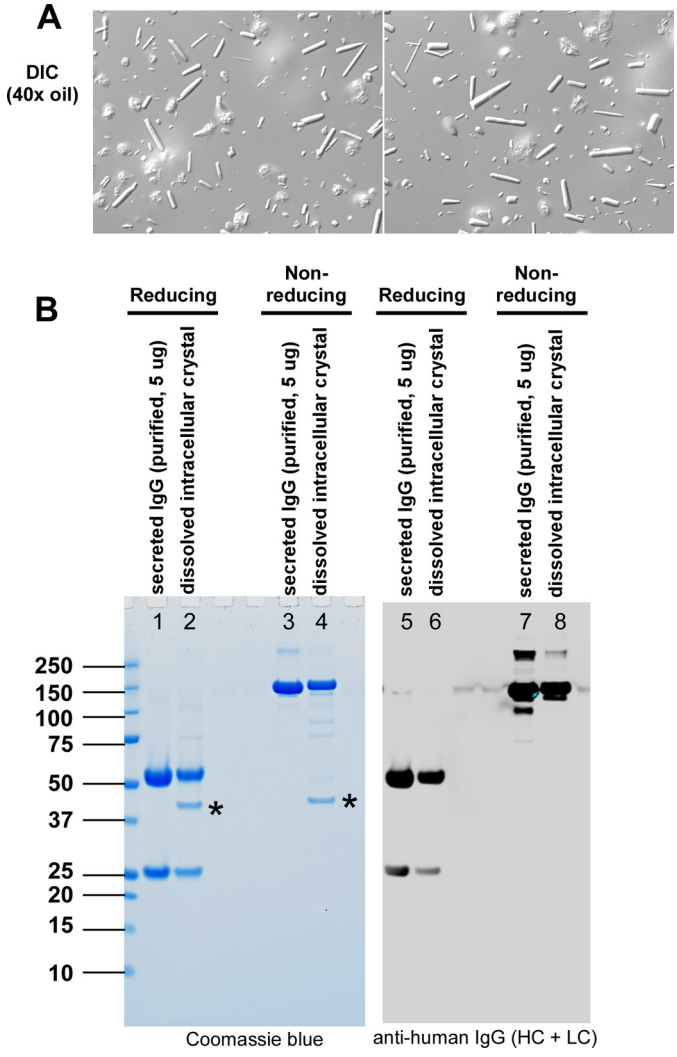

FIGURE 6. **Intra-ER crystals are composed of correctly assembled IgG.** *A*, intracellular crystals were isolated from detergent-extracted cell lysates (see "Experimental Procedures"). The quality of isolated crystals was assessed by DIC microscopy. *B*, both secreted IgG and dissolved intracellular crystals were resolved by SDS-PAGE under reducing and non-reducing conditions before staining with Coomassie Blue (*left panel*) or performing a Western blot (*right panel*) using an anti-human IgG antibody. A 40-kDa protein found in the crystal preparation (marked by *asterisks* in *lanes 2* and *4*) was mass spectrometrically identified to be hamster actin.

tribution of Golgi-resident enzymes to the ER (35) during the prolonged cell culture period. The results were again in good agreement with microscopy results showing that the crystals are housed in the ER.

To examine whether the crystal-forming IgG was folded properly, we assessed the expected function of IgG subdomains. To analyze the fold of CH2-CH3 domains, we tested whether the crystal-derived IgG could bind to staphylococcal protein A. Because the binding to protein A requires proper integrity of CH2-CH3 (36), a robust affinity purification of crystal-derived IgG by a widely used protein A resin method sufficiently demonstrated the proper folding and the integrity of CH2-CH3 domains (purification data are not shown, but the purified crystal-derived IgG was used in Fig. 8, *B* and *C*). To examine whether the Fab domains are correctly folded, we tested their ability to recognize cognate antigen via Western blotting (Fig. 8*B*). The electrotransferred antigen on a nitrocellulose membrane was probed either with protein A-purified IgG derived from crystals (Fig. 8*B*, *left panel*) or protein A-purified secreted IgG (Fig. 8*B*, *right panel*) at an identical antibody concentration. Western blotting results indicated that both IgGs were able to recognize their cognate antigens with equivalent efficiency. The results therefore implicated that the Fab domain of IgG derived from the intracellular crystals is folded and assembled equivalently to that of secreted IgG.

To obtain biophysical support on the fold and the stability of IgG, which contains 18 different intra- and interchain disulfide bridges per molecule, both secreted and crystal-derived IgGs were analyzed by differential scanning calorimetry (Fig. 8*C*). Whereas Fab and CH3 domains displayed equivalent thermal stability between the two compared IgGs, the melting temperature (T_m) of the glycan-bearing CH2 domain was ~4 °C lower in the crystal-derived IgG than that found in the secreted IgG. Our results hence highlighted that the core glycans added in the ER need to be further modified in the Golgi before the CH2 domain attains its full stability, but otherwise the gross fold of the crystal-derived IgG was largely equivalent to the secreted counterpart.

Physicochemical Properties of Model IgG Underscore Its Crystallizing Propensity—The calculated isoelectric point (pI) of our model IgG was pH 7.05, and the pI experimentally determined by capillary isoelectric focusing was around pH 7.4 (data not shown). The pH of the ER lumen, on the other hand, is reported to be around pH 7.2 in various cell types (37, 38). The coincidental proximity of pI to the pH of the ER lumen led us to hypothesize that this particular clone of human IgG has a propensity to form crystals at near neutral pH if the concentration is higher than a certain threshold. To test this hypothesis, we performed simple *in vitro* assays where a highly concentrated model IgG was exposed to near neutral pH in two different methods. The IgG was first purified to homogeneity from the harvested cell culture medium and was formulated in an acidic buffer (pH 5.2) at 105 mg/ml (antibody stock). In the first experiment, the antibody stock was subjected to an abrupt pH shift by adding [1.5/100] volume of 1 M citrate (pH 7.0). The moment the buffer pH was changed from pH 5.2 to near neutral, numerous crystals developed instantly and precipitated to the bottom of a glass vial (Fig. 9*A*, *right*). When the precipitates were examined by DIC microscopy, they were composed of rod-shaped crystals similar in appearance to the intra-ER crystals (Fig. 9*B*). When the *in vitro* generated crystals were analyzed by Raman spectroscopy, the Raman spectra exhibited signature peaks identical to those obtained from the intracellular crystals directly measured *in situ* (Fig. 9*D*). The evidence of Raman shift unequivocally showed that these two groups of crystals were composed of identical proteinaceous material. Under the conditions we used (*i.e.* 24-h static incubation at room temperature), the concentration of IgG that remained soluble in the aqueous phase was ~25 mg/ml IgG; therefore, 75% of IgG partitioned to the crystalline phase. Importantly, the results also implicated that no other proteinaceous factor was required for IgG crystallization in this *in vitro* pH shock experiment. In the second experiment, the antibody stock was dialyzed against PBS (pH 7.2) at 4 °C for 18 h to achieve a slower pH adjustment

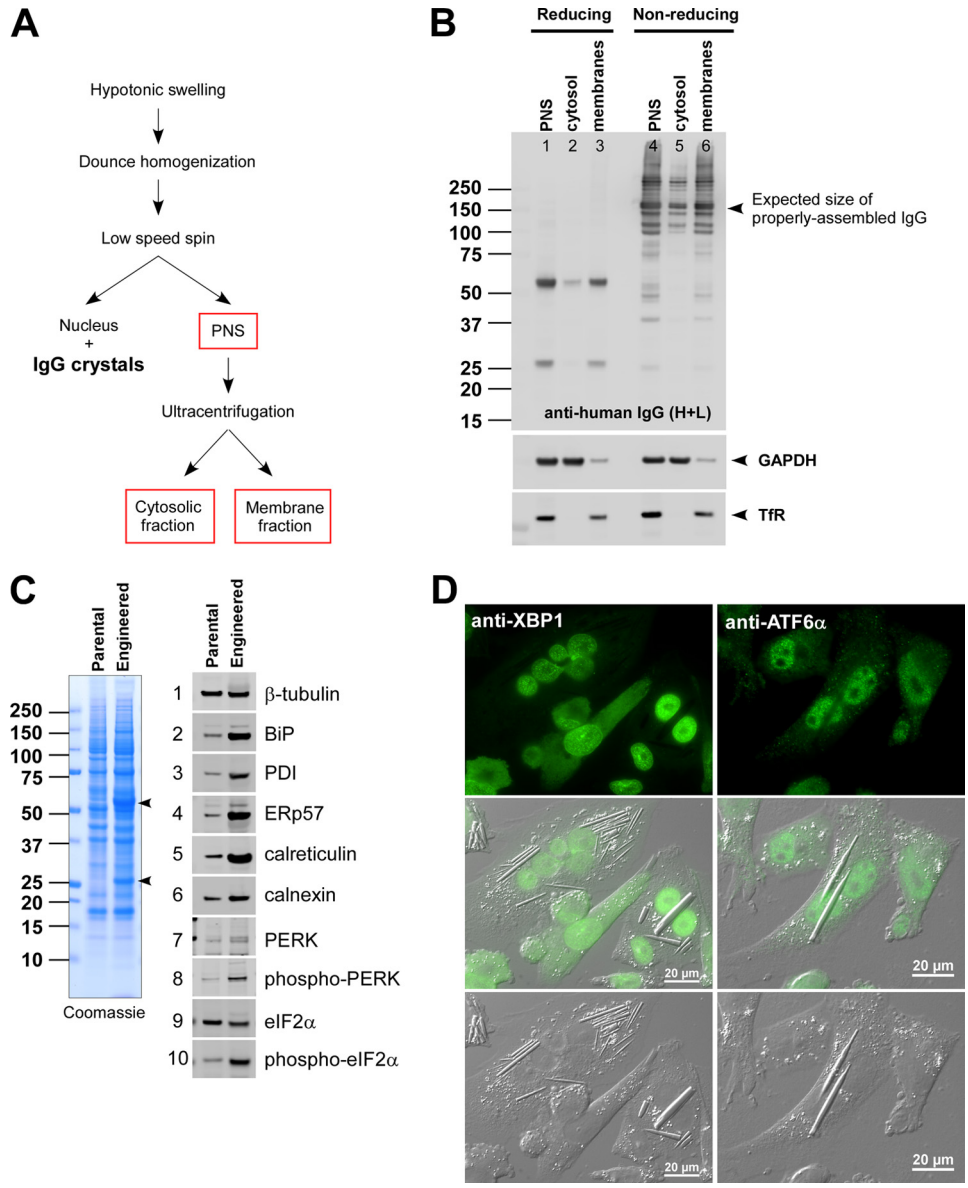

FIGURE 7. **Soluble milieu of ER contains various IgG folding intermediates.** *A*, a schematic of homogenization procedures used in this fractionation study. *B*, after the fractionation, samples were resolved by SDS-PAGE both under reducing and non-reducing conditions. Western blotting was performed by using anti-human IgG (HC + LC) (*top panel*), anti-GAPDH (*middle panel*), and anti-transferrin receptor (*TfR*) (*bottom panel*). *C*, a whole cell extract was prepared from parental CHO cells and the engineered CHO cells expressing model human IgG. The lysate representing 6×10^4 cells was loaded in each lane. *Left panel*, Coomassie staining of the whole cell lysates resolved under reducing conditions. *Right set* of *panels*, 10 selected proteins were detected by Western blotting. The names of the specific proteins are shown next to each blot. *D*, immunofluorescent staining of IgG-expressing engineered CHO cells with anti-XBP1 (*left set* of *panels*) or with anti-ATF6α (*right set* of *panels*). *Scale bars*, 20 μm. *PDI*, protein-disulfide isomerase.

from an acidic to a neutral range. Again, we observed crystalline precipitation during the dialysis. This time, however, much longer rod-shaped crystals had formed, and sometimes the crystals grew in a dendritic format (Fig. 9*C*). Again, a high enough concentration of fully assembled IgG placed in a near neutral pH environment was sufficient for the model IgG to nucleate crystals, and no additional proteinaceous factors were required for crystallization.

Neutralization of Acidic Cluster on Surface of CDR Abrogates Crystal-forming Propensity—The roles of pI and solution viscosity have been implicated in the crystallizing propensity of proteins (39, 40). However, the importance of these two attributes in our model IgG crystallization was not clear at first. There were numerous human IgG clones whose pI values fell near the pH of the ER lumen (pH 7.2) without exhibiting such crystal-forming propensity.[3] Although the solutions of our model IgG were viscous at high concentration (30 centipoises when measured at 141 mg/ml (pH 5.2)), there were some human IgG clones that exhibited higher viscosities but did not form crystals under similar testing conditions.[3] Therefore, the coincidental near neutral pI value or the high viscosity alone was insufficient to account for the *in vivo* and *in vitro* crystal-forming propensity.

To search additional physicochemical properties that may play roles in crystallizing propensity, the variable domain struc-

[3] R. Stevenson, H. Franey, and F. Kinderman, unpublished results.

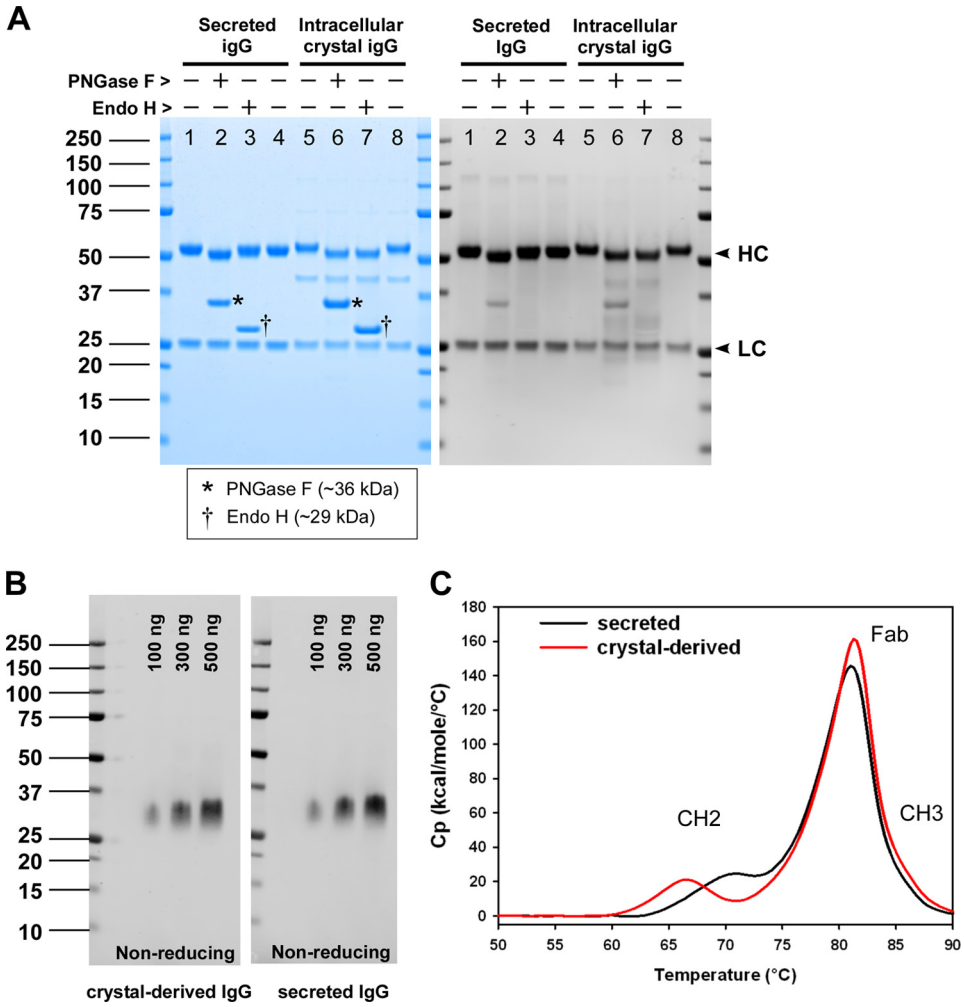

FIGURE 8. **IgG species derived from intra-ER crystals is folded correctly.** *A*, both secreted and intracellular crystal IgGs were treated with peptide:*N*-glycosidase F (*PNGase F*) or endo H. Enzyme-treated IgG was resolved by SDS-PAGE to examine the gel mobility under reducing conditions. HC and LC are indicated by the *arrowheads* shown on the *right* side of the gel. *Asterisks* are placed on *lanes 2* and *6* to mark peptide:*N*-glycosidase F. *Daggers* on *lanes 3* and *7* mark endo H. *B*, purified cognate antigen (100, 300, or 500 ng) was first resolved by SDS-PAGE under non-reducing conditions followed by an electrotransfer to a nitrocellulose membrane. The membrane was probed with protein A-purified IgG derived from intracellular crystals (*left panel*) or protein A-purified secreted IgG (*right panel*) at 1.6 μg/10 ml/blot. *C*, protein A-purified secreted IgG (*black line*) and protein A-purified crystal-derived IgG (*red line*) were formulated in acetate buffer (pH 5.2) and analyzed by differential scanning calorimetry. Heat capacity (*Cp*) is plotted on the *y axis* as a function of heat influx on the *x axis*.

ture of the IgG was computationally modeled and compared with a panel of other human IgGs produced in our laboratories (data not shown) and with the selected structural data available from Protein Data Bank (see Supplement 5 for three selected examples). Importantly, our model IgG exhibited a prominent negative charge patch (or a cluster of acidic residues) on the surface of the CDRs (Fig. 9*E*). The acidic cluster was composed of five aspartic acid residues all on the VH CDRs.[4] Because the prominent acidic cluster appeared to be an important, if not unique, property of this IgG clone, we hypothesized that the negative charge patch is directly contributing to the crystallizing propensity. To test this hypothesis, we mutated all five Asp residues into Ala (5D-to-5A) or Ser (5D-to-5S) simultaneously and examined their effects on viscosity and crystal-forming propensity using *in vitro* pH shift assays. Because we did not compensate for the loss of five negatively charged resides by introducing them back elsewhere in the same molecule (due to the apparent lack of appropriate permissive locations), the calculated pI of the resulting mutants significantly deviated from pH 7.05 (parent) to pH 8.54 (both mutants). Although the 5D-to-5A mutant resulted in 50% lower viscosity (15 centipoises measured at 157 mg/ml), the 5D-to-5S mutant exacerbated the viscosity roughly 100% (56 centipoises measured at 153 mg/ml). When the *in vitro* pH shock experiment was performed, neither mutant formed observable crystals at near neutral pH (data not shown). Because the three critical properties of the model IgG (*i.e.* pI, viscosity, and the acidic cluster) were closely linked to one another to give rise to the unique physicochemical properties, it was technically difficult to alter one isolated property without impacting the other two. Nonetheless, our mutagenesis study clearly demonstrated the importance of the acidic cluster in crystal-forming propensity at least *in vitro*. Because of the technical feasibility issues of expressing mutant IgGs under the identical syngeneic background by precisely replicating HC and LC gene copy num-

[4] R. Stevenson, H. Franey, F. Kinderman, T. Osslund, and R. R. Ketchem, unpublished results.

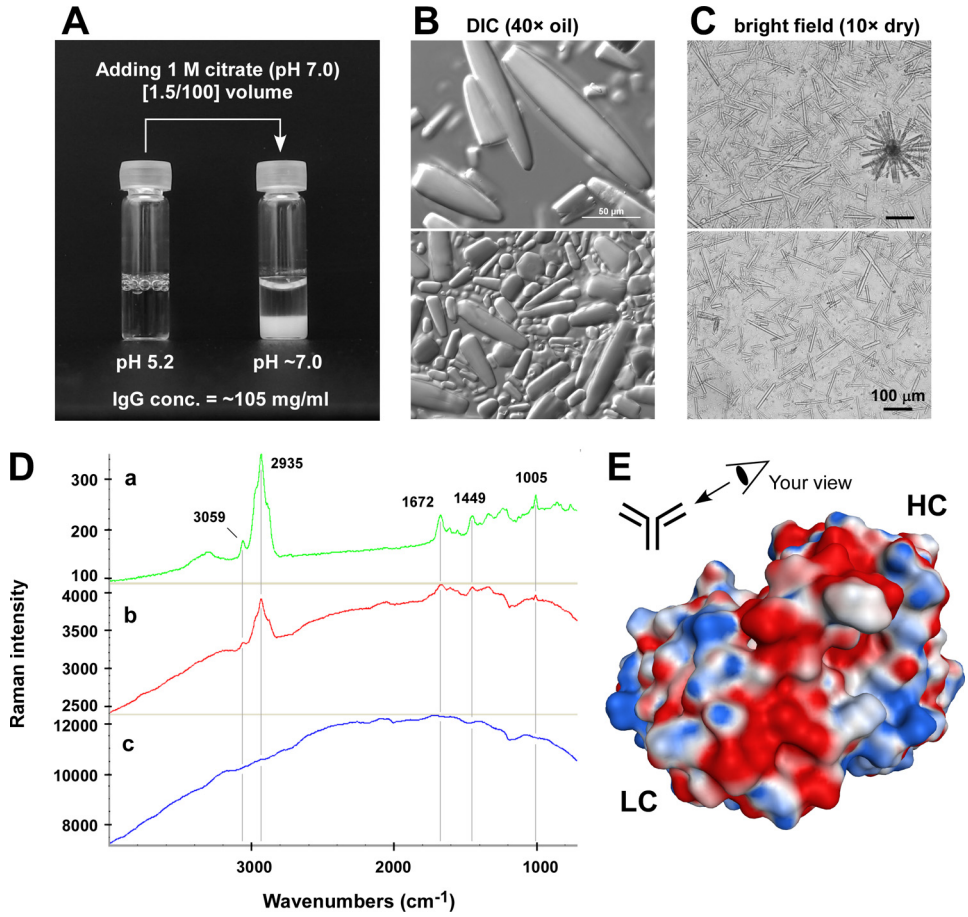

FIGURE 9. **Crystal-forming propensity is reproducible *in vitro*.** *A*, purified IgG was formulated in acetate buffer (pH 5.2) at 105 mg/ml. A [1.5/100] volume of 1 M citrate (pH 7.0) was added to the antibody stock to abruptly change the buffer pH to a neutral range. After the citrate addition, the IgG solution in a glass vial was incubated statically at room temperature for 24 h. After the incubation, the aqueous phase contained ~25 mg/ml IgG. *B*, crystals in the glass vial were examined using a DIC microscope with a 40× oil objective lens. *Scale bar*, 50 μm. *C*, purified IgG in acetate buffer was dialyzed against PBS (pH 7.2) for 18 h at 4 °C. Precipitates were collected and examined using a bright field microscope with a 10× dry objective lens. *Scale bar*, 100 μm. *D*, Raman spectra of crystals made from purified secreted IgG by pH shock procedures (*a*; *green*), crystals residing in the cytoplasm of paraformaldehyde-fixed intact cells (*b*; *red*), and the non-crystal-containing region of paraformaldehyde-fixed intact cells (*c*; *blue*). Representative signature spectra are indicated by wavelength *numbers* next to the peaks. *E*, computationally modeled Fv structure of the model IgG. The Fv is viewed from the perspective illustrated in the schematic. The surface model is color-coded by the underlying residue charge: *red* is negative, *blue* is positive, and *white* is neutral.

bers at exact multiple loci, we did not test whether the mutant IgGs would develop crystals intracellularly using stable CHO cell lines.

Blockade of Cargo Export from ER Induces IgG Crystallization in Transiently Transfected Cells—To compare wild type and mutant IgGs *in vivo* under an equivalent cellular background independent of transgene chromosomal integration sites or copy numbers, we expressed our model human IgGs in a fed batch transient expression system using HEK293-EBNA1 cells (22) in which "oriP"-containing expression vectors are episomally maintained in Epstein-Barr virus nuclear antigen 1-expressing HEK293 host cells. After a 6-day shaker flask cell culture following transfection, wild type and the two mutants accumulated 65–80 mg/liter secreted human IgG in the culture medium (Fig. 10*A*). However, throughout the 6-day suspension cell culture period, there was no evidence of intracellular crystal development (not shown). Evidently, the rate of protein synthesis and protein folding did not exceed the ER export efficiency at steady state in this transient expression system under the conditions used.

To test whether slowing down the rate of ER export is sufficient to cause enough accumulation of fully folded IgG in the ER lumen and lead to crystal formation, we treated transiently transfected HEK293 cells with brefeldin A (BFA) for 24 h, from day 2 to 3 post-transfection, using a fresh culture medium. As expected, the BFA treatment largely blocked the secretion of IgG from transfected cells during the 24-h period (Fig. 10*B*). Intracellular crystals became detectable in nearly 30% of the cells that express HC and LC of the wild type IgG after 24-h BFA treatment (Fig. 10*C*, *left two columns*, *top row*). No crystal was detectable without the BFA treatment (Fig. 10*C*, *right two columns*, *top row*). The cells expressing mutant IgGs did not develop crystals under identical conditions regardless of BFA treatment (Fig. 10*C*, *middle* and *bottom rows*). The results not only suggested that the removal of the acidic patch abrogates the crystallization propensity *in vivo* but also that even when the rate of recombinant protein synthesis is low, if we block the cargo export from the ER, the transfected cells can accumulate enough properly folded IgG above a threshold concentration in the ER lumen to nucleate intracellular crystals. In other words,

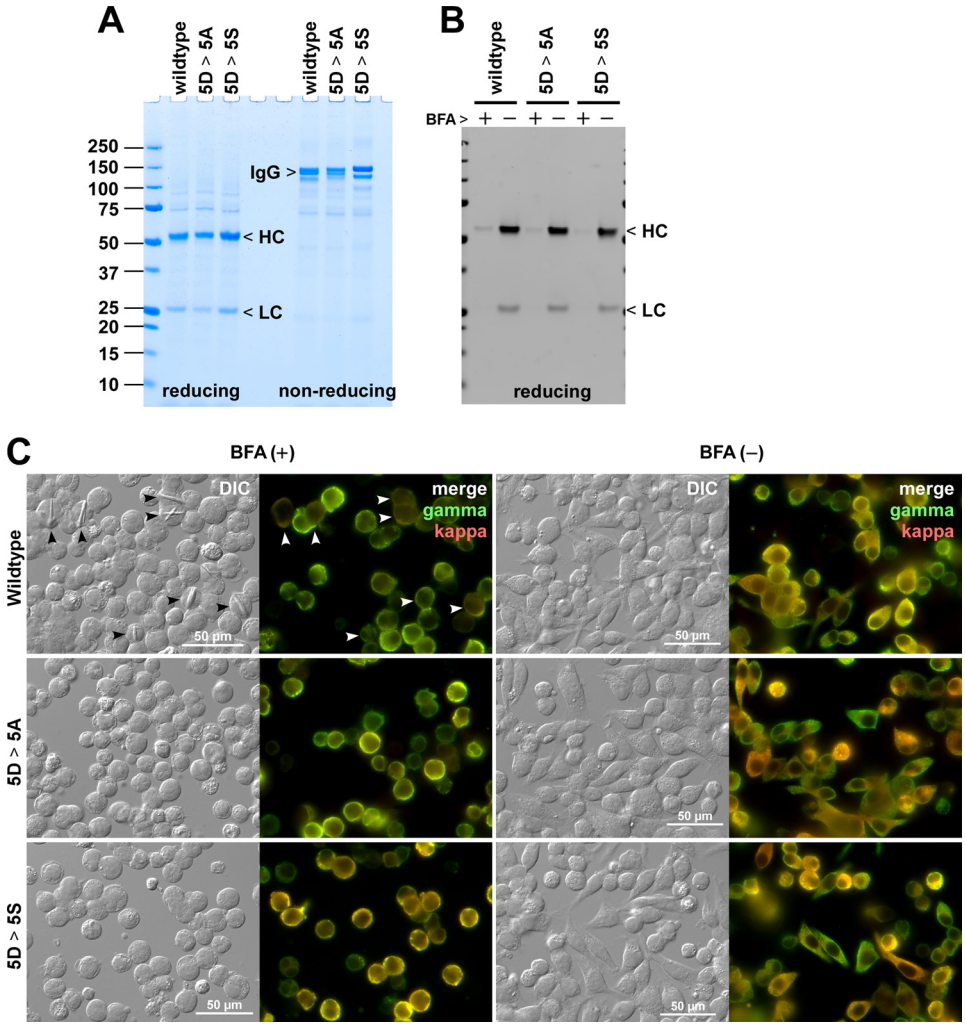

FIGURE 10. **Transiently transfected HEK293 cells develop intracellular crystals when ER export is blocked by brefeldin A.** *A*, HEK293 cells were transiently transfected with IgG-encoding expression vectors. On day 6 post-transfection, cell culture media were harvested, and the protein quality was analyzed by SDS-PAGE under reducing and non-reducing conditions. A sample equivalent to 5 μl of neat culture medium was loaded per lane. The expression titer was 75 mg/liter for wild type IgG, 66 mg/liter for the 5D-to-5A mutant (*5D > 5A*), and 81 mg/liter for the 5D-to-5S mutant (*5D > 5S*). *B*, BFA treatment blocks IgG secretion. Transfected cells were cultured in a fresh medium from day 2 to day 3 post-transfection for 24 h either in the presence or absence of 15 μg/ml brefeldin A. The amount of IgG secreted to the culture medium during the 24-h period was examined by Western blotting after resolving the proteins by SDS-PAGE under reducing conditions. *C*, on day 2 post-transfection, the cells were seeded onto glass coverslips and cultured statically for 24 h in the presence (*left two columns*) or the absence (*right two columns*) of 15 μg/ml BFA. On day 3 post-transfection, the cells were fixed with paraformaldehyde, permeabilized, and immunostained with FITC-conjugated goat anti-γ chain and Texas Red-conjugated goat ant-κ chain antibodies. The wild type IgG-expressing cells that developed detectable intracellular crystals are marked by *arrowheads*. The "*merge*" is a digital overlay of anti-γ staining (*green*) and anti-κ staining (*red*). Crystals developed only in cells expressing wild type IgG under BFA treatment. *Scale bars*, 50 μm.

when the crystals appear in the cells, the ER export steps have become rate-limiting relative to those of protein synthesis and oxidative protein folding.

DISCUSSION

During human IgG overexpression, our engineered CHO cell line developed a striking phenotype where cells nurtured intracellular crystals accompanied by cell growth and karyokinesis in the absence of cytokinesis. To understand what caused this peculiar phenotype, we first identified the composition and the subcellular localization of the crystals. The crystals were composed of human IgG and resided in the ER lumen. When isolated and dissolved, the IgG derived from the intra-ER crystals was sensitive to endo H but correctly assembled and fully folded, and it retained antigen binding ability; thus, it technically had the attributes considered to be "exportable" from the ER. The export-ready IgGs nonetheless accumulated in the ER lumen. One way to explain this observation is to postulate a lack of sufficient capacity at the ER exit sites to concentrate and package export-ready IgG into COP II vesicles. Alternatively, the protein synthesis and oxidative folding efficiency might have far exceeded the ER export trafficking capacity. The net results are the progressive build-up of export-ready IgG in the ER lumen. Based on the identified unique propensities that result in instantaneous crystallization at high concentration at near neutral pH, we propose that the export-ready IgG progressively accumulated in the ER until the crowding reached a threshold concentration to nucleate IgG crystals. In essence, the intra-ER crystal nucleation precisely reports the accumulation of export-ready IgG above a threshold concentration. Once the crystals formed, intra-ER crowding was alleviated as we observed in markedly reduced IgG staining signals in crys-

tal-harboring cells. This hypothetical model would suggest that the newly folded IgG molecule faces two alternative intracellular fates, namely either becoming part of the growing crystals in the ER or being exported out of the ER, trafficked to the Golgi, and then secreted.

Given that the CHO cells of normal size with a single nucleus were already developing crystals, we propose that cell enlargement and formation of syncytia occurred after the crystal nucleation. The growing intra-ER crystals perhaps inhibited the normal progression of cytokinesis by physically disrupting certain steps of coordinated sequential events. As a result, cells became larger *as if* to nurture the crystal growth until cells were damaged by membrane puncture when the elongating ends of crystals breached the integrity of membranes.

Phenotype variations among the cells in a clonal population are widely observed (41). In the clonal population of recombinant CHO cells we studied, some cells developed crystals early, some cells developed crystals late, and others did not develop crystals during a defined time window of cell cultivation period despite that all the cells expressed and secreted the same human IgG clone. This observation clearly suggested that the mere overexpression of IgG with the peculiar physicochemical properties alone was not sufficient to produce this extreme cellular phenotype. During the cell line development stages, for example when the cells were maintained in stringent selection media, we did not observe intracellular crystals (data not shown). Furthermore, when the model IgG was expressed using a transient expression platform, crystals failed to develop in the ER lumen unless ER-to-Golgi transport was blocked to accumulate export-ready IgG in the ER. We propose that, even with the unique propensity, the intra-ER crystal nucleation would not take place unless the nascent chain input and folding efficiency exceed the ER export capacity to accumulate fully assembled IgG species above a threshold concentration. We speculate that extensive efforts in the optimization of expression vectors, CHO cell hosts, culture media, and cell growth conditions all played roles to attain high biosynthetic capabilities that surpassed the ER export capacity even at steady-state cell growth conditions.

Because highly purified model IgG can instantly form crystals upon pH shift to a neutral range without a need for additional factors, we propose that the high local concentration of fully folded IgG is the sole trigger required for the crystal nucleation and subsequent growth in the ER lumen. Because the molecular packing at a neutral pH appeared to be instantaneous, we hypothesize that there are strong intermolecular forces that govern IgG self-alignment and packing. Based on the results of mutagenesis, we propose that the clustered negatively charge residues on the CDR surface played critical roles in coordinating dipole-dipole interactions and facilitated near instant IgG self-assembly.

Unlike the accumulation of unfolded/misfolded proteins that causes a severe ER stress, documentation on the accumulation of properly folded protein in the ER of animal cells is scarce. In contrast, plant cells can naturally accumulate proteins in the ER without causing a severe ER stress that can kill the afflicted cells. During the seed maturation process of cereal plants such as rice, maize, and wheat, the plants use the ER to accumulate nutritionally important proteins in the form of large protein aggregates called protein bodies (42), and thus their ER is often termed as storage ER. In these plant cells, controlled aggregation of particular classes of proteins (*e.g.* γ-zein, γ-gliadin, etc.) is proposed to be a mechanism of escaping the ER-associated degradation and accumulating a massive amount of proteins in the ER lumen without causing severe ER stress (42). Because our recombinant messages encoding IgG HC and LC were designed to be translated by a cap-dependent ribosomal scanning mechanism, we expected the translation to stall if the cells were undergoing a severe ER stress that activates PERK, which in turn phosphorylates eIF2α (43). To the contrary, although the overexpression of IgG itself activated all three arms of UPR signaling pathways constitutively, the IgG synthesis appeared to continue, and the newly folded IgG kept feeding into the elongating crystals until crystals outgrew the cell size and eventually breached the membranes. Thus, similar to protein bodies in cereal plants, the intra-ER IgG crystals did not apparently expose the ER to extensive stress during their inception and growth. One important consequence of UPR activation is apoptosis when the cells cannot cope with the burden of protein folding demand; however, we did not observe a sign of acute cell health deterioration during the cell culture. We propose that the engineered CHO cells manage the ER stress effectively by up-regulating protein folding capacity by activating UPR pathways. In other words, the intrinsic plasticity of CHO cells allowed the adaptation to a higher biosynthetic load by changing the cellular phenotype to meet the ongoing demand.

In bacteria, inclusion bodies often form when exogenous proteins are overexpressed (44). Unlike bacterial inclusion bodies, which are composed of terminally misfolded, refractory insoluble aggregates, the intra-ER IgG crystals dissolved completely when the local IgG concentration was lowered. Besides, the IgG crystals were composed of properly assembled and correctly folded IgG species that retained antigen binding abilities. Our intra-ER crystals were also clearly distinct from the "aggresomes," which form in the cytosol to sequester misfolded proteins to the juxtanuclear region (45, 46).

Protein folding and structural maturation in the ER have long been generally considered slow and inefficient (47, 48). Our observation using a "non-professional" secretory cell (CHO) that expresses an exogenous secretory cargo (human IgG) implicated that the ER export steps were more rate-limiting than the protein folding and assembly steps at least for this particular human IgG clone. Because the intra-ER crystal formation potentially competes with ER export machinery to gain access to the new supply of fully folded IgGs, our results indicated that intra-ER IgG crystals are "excess inventory" that could have been secreted if the ER exit sites had higher functional capacity. There could be multiple mechanisms that rendered the ER export steps rate-limiting. For example, an imbalance between anterograde and retrograde traffic resulting from the high secretory activities might have depleted the forward moving trafficking machinery at the ER exit sites. The absolute number of cellular machinery (*e.g.* cargo receptors, coat subunits, SNAREs, tethers, rabs, etc.) might have simply been insufficient. The supply of ATP might have been limiting to fuel

catalytic reactions. Alternatively, given that our CHO cell hosts are typically capable of secreting other human IgG clones at a much higher specific productivity (qP), which typically yields higher volumetric secretion titers sometimes reaching 5–10 g/liter (data not shown), some unknown intrinsic properties of our model IgG clone might have rendered the interaction with ER export machinery inefficient.

A precise understanding of the intracellular trafficking bottlenecks that created this cellular phenotype will nonetheless enable us to find ways to rescue the phenotype and to increase cellular secretory capacity further. Whether such bottlenecks are specific to this particular human IgG clone or applicable to other secretory cargoes in general awaits further investigation. What is clear, however, is that the detailed mechanistic understanding of this critical transport step could lead to viable strategies that enhance secretory pathway functions and maximize the use of cellular capacity. This in turn will lead to more cost-effective manufacturing of therapeutically important glycoproteins that not only benefit patients who use biopharmaceutics but also the parties who subsidize the associated medical costs. The ER exit site functions and the ER-to-Golgi transport steps are one of the most extensively investigated areas in protein/membrane trafficking cell biology. Translating the accumulated mechanistic knowledge into biopharmaceutical production by accelerating this critical rate-limiting step will be our immediate future challenges.

Acknowledgments—We thank Kevin Graham and Rick Jacobsen for help in expression vector construction and Jill Cai and Lynette Buck for the effort in stable cell line development. We also thank Bram Estes and Carolyn Chu for producing and purifying IgG mutants, respectively, via transient transfection as well as Henry Lin for useful discussion. We are indebted to Craig Zupke, Jeffery McGrew, and Wei Yan for critical input. We extend our thanks to Randolph Mohr for consultation on legal and proprietary matters.

REFERENCES

1. Brewer, J. W., and Hendershot, L. M. (2005) *Nat. Immunol.* **6,** 23–29
2. Durocher, Y., and Butler, M. (2009) *Curr. Opin. Biotechnol.* **20,** 700–707
3. Dinnis, D. M., and James, D. C. (2005) *Biotechnol. Bioeng.* **91,** 180–189
4. Jenkins, N., Murphy, L., and Tyther, R. (2008) *Mol. Biotechnol.* **39,** 113–118
5. Arvan, P., Zhao, X., Ramos-Castaneda, J., and Chang, A. (2002) *Traffic* **3,** 771–780
6. Ellgaard, L., Molinari, M., and Helenius, A. (1999) *Science* **286,** 1882–1888
7. Lee, J., Lau, J., Chong, G., and Chao, S. H. (2007) *Biotechnol. Lett.* **29,** 1797–1802
8. Barnes, L. M., and Dickson, A. J. (2006) *Curr. Opin. Biotechnol.* **17,** 381–386
9. Lucas, B. K., Giere, L. M., DeMarco, R. A., Shen, A., Chisholm, V., and Crowley, C. W. (1996) *Nucleic Acids Res.* **24,** 1774–1779
10. Williams, S., Mustoe, T., Mulcahy, T., Griffiths, M., Simpson, D., Antoniou, M., Irvine, A., Mountain, A., and Crombie, R. (2005) *BMC Biotechnol.* **5,** 17
11. Wang, T. Y., Yang, R., Qin, C., Wang, L., and Yang, X. J. (2008) *Cell Biol. Int.* **32,** 1279–1283
12. Mariati, Ho, S. C., Yap, M. G., and Yang, Y. (2010) *Protein Expr. Purif.* **69,** 9–15
13. Alete, D. E., Racher, A. J., Birch, J. R., Stansfield, S. H., James, D. C., and Smales, C. M. (2005) *Proteomics* **5,** 4689–4704
14. Peng, R. W., Guetg, C., Tigges, M., and Fussenegger, M. (2010) *Metab. Eng.* **12,** 18–25
15. Tigges, M., and Fussenegger, M. (2006) *Metab. Eng.* **8,** 264–272
16. Jenkins, N., Meleady, P., Tyther, R., and Murphy, L. (2009) *Biotechnol. Appl. Biochem.* **53,** 73–83
17. Müller, D., Katinger, H., and Grillari, J. (2008) *Trends Biotechnol.* **26,** 359–365
18. Shukla, A. A., and Thömmes, J. (2010) *Trends Biotechnol.* **28,** 253–261
19. O'Callaghan, P. M., and James, D. C. (2008) *Brief. Funct. Genomic. Proteomic.* **7,** 95–110
20. Aldrich, T. L., Thomas, J. N., and Morris, A. E. (1998) *Cytotechnology* **28,** 9–17
21. Rasmussen, B., Davis, R., Thomas, J., and Reddy, P. (1998) *Cytotechnology* **28,** 31–42
22. Durocher, Y., Perret, S., and Kamen, A. (2002) *Nucleic Acids Res.* **30,** E9
23. He, F., Hogan, S., Latypov, R. F., Narhi, L. O., and Razinkov, V. I. (2010) *J. Pharm. Sci.* **99,** 1707–1720
24. Altschul, S. F., Gish, W., Miller, W., Myers, E. W., and Lipman, D. J. (1990) *J. Mol. Biol.* **215,** 403–410
25. Berman, H. M., Westbrook, J., Feng, Z., Gilliland, G., Bhat, T. N., Weissig, H., Shindyalov, I. N., and Bourne, P. E. (2000) *Nucleic Acids Res.* **28,** 235–242
26. Kabat, E. A., Wu, T. T., and Bilofsky, H. (1977) *J. Biol. Chem.* **252,** 6609–6616
27. Hawi, S. R., Nithipatikom, K., Wohlfeil, E. R., Adar, F., and Campbell, W. B. (1997) *J. Lipid Res.* **38,** 1591–1597
28. Gipson, I. K., Burns, R. P., and Wolfe-Lande, J. D. (1975) *Invest. Ophthalmol.* **14,** 937–941
29. Tagliavacca, L., Anelli, T., Fagioli, C., Mezghrani, A., Ruffato, E., and Sitia, R. (2003) *Biol. Chem.* **384,** 1273–1277
30. Ortsäter, H., and Sjöholm, A. (2007) *Mol. Cell. Endocrinol.* **277,** 1–5
31. Rutkowski, D. T., and Kaufman, R. J. (2004) *Trends Cell Biol.* **14,** 20–28
32. Yoshida, H., Matsui, T., Yamamoto, A., Okada, T., and Mori, K. (2001) *Cell* **107,** 881–891
33. Yoshida, H., Oku, M., Suzuki, M., and Mori, K. (2006) *J. Cell Biol.* **172,** 565–575
34. Haze, K., Yoshida, H., Yanagi, H., Yura, T., and Mori, K. (1999) *Mol. Biol. Cell* **10,** 3787–3799
35. Klausner, R. D., Donaldson, J. G., and Lippincott-Schwartz, J. (1992) *J. Cell Biol.* **116,** 1071–1080
36. Deisenhofer, J. (1981) *Biochemistry* **20,** 2361–2370
37. Casey, J. R., Grinstein, S., and Orlowski, J. (2010) *Nat. Rev. Mol. Cell Biol.* **11,** 50–61
38. Paroutis, P., Touret, N., and Grinstein, S. (2004) *Physiology* **19,** 207–215
39. Hand, D. B. (1935) *J. Gen. Physiol.* **18,** 847–852
40. Kantardjieff, K. A., and Rupp, B. (2004) *Bioinformatics* **20,** 2162–2168
41. Pilbrough, W., Munro, T. P., and Gray, P. (2009) *PLoS One* **4,** e8432
42. Vitale, A., and Ceriotti, A. (2004) *Plant Physiol.* **136,** 3420–3426
43. Harding, H. P., Zhang, Y., and Ron, D. (1999) *Nature* **397,** 271–274
44. Carrió, M. M., and Villaverde, A. (2002) *J. Biotechnol.* **96,** 3–12
45. Kopito, R. R. (2000) *Trends Cell Biol.* **10,** 524–530
46. Markossian, K. A., and Kurganov, B. I. (2004) *Biochemistry* **69,** 971–984
47. Ellgaard, L., and Helenius, A. (2003) *Nat. Rev. Mol. Cell Biol.* **4,** 181–191
48. Sitia, R., and Braakman, I. (2003) *Nature* **426,** 891–894